General Disclaimer

One or more of the Following Statements may affect this Document

- This document has been reproduced from the best copy furnished by the organizational source. It is being released in the interest of making available as much information as possible.

- This document may contain data, which exceeds the sheet parameters. It was furnished in this condition by the organizational source and is the best copy available.

- This document may contain tone-on-tone or color graphs, charts and/or pictures, which have been reproduced in black and white.

- This document is paginated as submitted by the original source.

- Portions of this document are not fully legible due to the historical nature of some of the material. However, it is the best reproduction available from the original submission.

Produced by the NASA Center for Aerospace Information (CASI)

NASA Technical Memorandum 87080

Optical Analysis of Parabolic Dish Concentrators for Solar Dynamic Power Systems in Space

Kent S. Jefferies
Lewis Research Center
Cleveland, Ohio

August 1985

NASA

OPTICAL ANALYSIS OF PARABOLIC DISH CONCENTRATORS FOR

SOLAR DYNAMIC POWER SYSTEMS IN SPACE

Kent S. Jefferies
National Aeronautics and Space Administration
Lewis Research Center
Cleveland, Ohio 44135

SUMMARY

Solar dynamic power systems are currently being considered as an electric power source for the proposed Space Station. A major advantage of solar dynamic systems is the reduction in area for collecting solar energy to about 1/3 or 1/4 that of photovoltaic arrays. This significantly increases the field of view from the Space Station, enables easier access to the station, and reduces the amount of propellant required to maintain Space Station altitude, particularly since the station will be orbiting in low earth orbit (LEO). In addition, solar concentration has the potential to provide large quantities of thermal power for manufacturing processes in space. Where heat energy is required, it is several times more efficient to collect thermal energy directly than to use electric-resistance heating.

An optical analysis of a parabolic solar collection system operating in earth orbit was performed using ray tracing techniques. The analysis included the effects of:

(1) Solar limb darkening
(2) Parametric variation of mirror surface error
(3) Parametric variation of mirror rim angle
(4) Parametric variation of alignment and pointing error

This ray tracing technique used numerical integration to combine the effects of rays emanating from different parts of the sun at different intensities with the effects of normally-distributed mirror-surface errors to compute the angular intensity distribution of rays leaving the mirror surface. A second numerical integration was then performed over the surface of the parabolic mirror to compute the radial distribution of brightness at the mirror focus.

Major results of the analysis included:

(1) Solar energy can be collected at high temperatures with high efficiency. For example, using a parabolic mirror of 60° rim angle that has a specular reflectivity of 0.9 and a surface error of 2 milliradians standard deviation, the net power into an absorber at 1100 K (1500 °F) is 86 percent of the solar power intercepted by the mirror.

(2) Higher absorber temperatures can be achieved at lower efficiencies, or higher efficiencies can be achieved at lower temperatures. Both temperature and efficiency can be increased by increasing mirror surface accuracy and/or mirror spectral reflectivity.

(3) Collection efficiency is near its maximum level across a broad plateau of rim angles from 40° to 70°. At lower rim angles, the cause of reduced efficiency is an increase in distance from the mirror to its focus; at higher rim angles, efficiency falls off because rays from the mirror's rim impinge on the focal plane at grazing angles.

INTRODUCTION

Solar dynamic power systems are currently being considered as an electric power source for the proposed Space Station. A major advantage of solar dynamic systems is the reduction in area for collecting solar energy to about 1/3 or 1/4 that of photovoltaic arrays. This significantly increases the field of view from the Space Station, enables easier access to the station, and reduces the amount of propellant required to maintain Space Station altitude, particularly since the station will be orbiting in low earth orbit (LEO). In addition, solar concentration has the potential to provide large quantities of thermal power for manufacturing processes in space. Where heat energy is required, it is several times more efficient to collect thermal energy directly than to use electric-resistance heating.

Current-technology Rankine, Brayton, and Stirling space power systems require high temperature (600 to 1100 K) thermal input. Advanced-technology Rankine, Brayton, and Stirling power systems may achieve superior performance with thermal input temperatures up to 1500 K. Solar dynamic systems require concentration of sunlight to produce these temperatures. Achievable temperatures and efficiencies are a function of the concentrator geometry, alignment and tracking errors, mirror surface accuracy, and spectral reflectance.

The analysis reported herein determines what efficiencies and temperatures are feasible and what mirror optical characteristics are required to achieve these performances. It is an optical analysis of sunlight focused by a parabolic mirror into an absorber orifice with blackbody re-radiation at the absorber temperature. Analysis of the solar absorber itself and of thermal transport and distribution systems was not included in this study, but would be needed to determine overall concept feasibility.

Previous analyses of parabolic concentration for powering heat engines to generate electric power in space were done in the early 1960's (refs. 3, 10, 17, and 33). Some of these analyses (such as ref. 10) used methods and assumptions similar to those of the analysis reported herein. Results of these early analyses generally are in close agreement with this current analysis. However, this analysis, benefiting from increased computer capability, was able to examine more cases and produce more comprehensive results than were achieved in the earlier analyses of space concentrators. This increased computer capability also enabled the inclusion of solar limb darkening. Additional analyses have been performed in the late 1970's and early 1980's in support of terrestrial solar power systems. These terrestrial analysis included such terrestrial phenomena as reduced solar intensity, intermittent illumination, and atmospheric scattering. Thus, their results are not directly relevant to solar collection in space.

A parabolic concentration system consists of several components which together determine the energy collection efficiency of the system and the attainable temperature; namely, the sun, the mirror, the absorber, and the

alignment and pointing system. This analysis studied each component and evaluated how the components individually and collectively influence system performance.

ANALYSIS METHOD

Light rays were traced from different areas of the sun to the parabolic mirror and then from subdivisions of the mirror to annular subdivisions of the focal plane. Brightness variations from the center to the less bright edge of the sun (ref. 1), known as solar limb darkening, were accounted for in the intensities of the rays leaving the sun. Numerical integration was used to combine these intensities with a two-dimensional normal distribution of mirror surface errors to determine the angular intensity distribution of rays leaving the mirror. These intensities were then multiplied by the assumed 90 percent reflectivity of the mirror.

A second numerical integration (over the surface of the mirror) was performed to determine the brightness of each subdivision of the focal plane. A third numerical integration was used to determine the flux in annular regions of an absorber orifice displaced due to alignment and pointing errors from the center of the focus. Blackbody radiation at the assumed absorber cavity temperature was subtracted from the radiation entering the cavity to calculate net power into the absorber. Overall collection efficiency was calculated by dividing net power into the absorber by total power intercepted by the primary mirror. This enables evaluation of various collection system designs.

Solar Limb Darkening

The center of the sun is about 50 percent brighter than the edge of the sun. This brightness variation is due primarily to the fact that the sun consists of layers of radiating gases rather than a well-defined surface. The Astrophysical Observatory of the Smithsonian Institute has precisely measured the energy distribution over the solar disk. Angstrom and Angstrom (ref. 1) approximated this energy distribution by the following formula:

$$I = I_o (1. - 0.342 \, d^{2.4}) \tag{1}$$

where I is the energy intensity at distance d (radii) from the center of the sun ($0 \leq d \leq 1$). I_o is the intensity at the center of the solar disk. This formula is plotted in figure 1.

Assuming the mirror to be in Earth orbit, "air mass zero" solar flux of 1.371 (kW/sq m) (ref. 24) was used in this analysis. The following equation was derived by integrating equation (1) to represent the solar flux (F) from each 2 percent radius increment solar annulus. (The sun was divided into 50 2 percent radius annuli for the numerical integration.)

$$F = 1.371(2.368 - 0.81 \, d^{2.4}) \, 0.02 \, d \tag{2}$$

The solar flux in each 2 percent radius increment solar annulus computed from equation (2) is plotted in figure 2.

Mirror Surface Errors

This analysis assumed a two-dimensional normal circular probability distribution of mirror surface error. The standard deviation of this distribution was parameterized using values of 0, 0.0005, 0.001, 0.002, and 0.005 rad. The mirror surface error is the local angular deviation of the mirror surface from the ideal paraboloid. The resulting deviation in the reflected ray as shown on figure 3 is twice the mirror surface error. The two-dimensional normal probability distribution is represented by the formula:

$$\sigma P(\epsilon) = (\epsilon/\sigma)e^{-0.5\epsilon^2/\sigma^2}$$

in which $P(\epsilon)$ is the probability density of error ϵ, σ is the standard deviation, and e is the base of natural logarithms. This equation is plotted in figure 4.

Mirror Geometry

The second numerical integration in this analysis integrated intensity distributions from segments of the parabolic mirror. The distance from each segment to the focus and the angle with which each ray approaches the absorber orifice were taken into account.

Alignment and Pointing Errors

This analysis assumed that the collection system would be designed to operate at full power with a given maximum alignment and pointing error. The maximum error was varied parametrically with four values of misorientation (2.5, 5.0, 7.5, and 10.0 milliradians). For each of these values, the flux falling on annular regions of an absorber orifice misoriented from the image of the sun was calculated by numerical integration.

RESULTS

Optimum system geometry and the overall system performance are governed by the errors inherent to each component comprising the system. The sun, although not truly a part of the collection system, limits the attainable collection efficiency because it provides a limited thermal flux and is a radiating gaseous sphere rather than a point source. The mirror absorbs part of the solar energy, and because it is not a perfect paraboloid, slightly misdirects the reflected energy. Collection efficiency is also influenced by the "rim angle" of the mirror, which is the angle between the mirror axis and a line from the focus to the mirror rim. The absorber orifice is the entrance for solar radiation into the absorber cavity, but it also allows radiation to escape. Errors in alignment and pointing cause less of the solar energy to enter the absorber and thereby reduce collection efficiency. The following discussion and figures show the impacts of each of these factors on system performance.

Angular Flux Distribution Leaving Mirror

The first integration computed the intensities of reflected rays based on their angular deviation from an ideal ray reflected towards the center of focus. The angular deviation of each reflected ray is the vector sum of the angular deviation of the source of the ray from the center of the sun plus twice the angular deviation of the portion of the mirror reflecting the rays from a perfect parabola. Figure 5 shows curves of flux leaving the mirror surface versus angular deviation for mirror surface errors with standard deviations of 0.0, 0.5, 1.0, 2.0, and 5.0 milliradians. These standard deviations apply to both the radial and the tangential components of the two-dimensional normal circular probability distribution of mirror surface error. The 0 milliradian curve is the same as the curve on figure 2 except for the 10 percent of the flux that was absorbed at the mirror surface.

The curve with 0.5 milliradians of mirror surface standard error is quite similar, showing a slightly lower peak flux and a tailing off less abrupt than the dropoff of the 0 milliradian curve. Above 1 milliradians of mirror surface standard error, both the angular dispersion of sunlight and the mirror surface errors are important in determining the resulting dispersion of the reflected flux. Five milliradians of mirror-surface standard error drastically spreads the reflected flux.

Radial Distribution of Power at the Focal Plane

Radial distribution of power at the focal plane represents the output of concentrator optics and the input to absorber thermodynamics. The angular distribution of flux leaving the mirror and the distance and angle from each portion of the mirror to the focus determine the power distribution at the focal plane. Variations of this distribution with mirror geometry parameters enable optimization of the mirror geometry. This power distribution also influences absorber design by showing what power intensities the absorber must accommodate.

Curves of the percent of power in each one-thousandth mirror diameter annulus are plotted in figure 6. The curves are for 0.0, 0.5, 1.0, 2.0, and 5.0 milliradians standard deviation, two-dimensional normal circular probability distribution of mirror surface error. The curves are quite similar to the curves of angular distribution of flux leaving the mirror which were plotted on figure 5. The scaling is different from figure 5 in that different variables are plotted on the axes.

The important difference between figures 5 and 6 is that figure 6 includes the effects of mirror geometry. Flux from the rim of the mirror travels further and strikes the focus more obliquely than flux from the center of the mirror. The effect of this is most noticeable on the curve with no mirror surface error. On figure 5, the curve dropped to zero abruptly after reaching its peak. On figure 6, the curve starts down abruptly, but then approaches the x-axis asymptotically. The initial dropoff on figure 6 corresponds to the edge of the sun's image reflected from the center of the mirror. The sun's images from other parts of the mirror extend out into the tapering off region of this curve.

5

Brightness of Annular Regions of Focal Plane

The flux in figure 5 and the power in figure 6 are based on annular regions, which increase in size proportional to the radius. The power per unit area or brightness of the annular regions around the focus is plotted in figure 7. The curves are plotted as a function of the ratio of focus diameter to mirror diameter in order for the results to be independent of mirror diameter.

In figure 7, the curve for zero standard error is shaped by two factors: the distribution of brightness over the solar disk and the obliquity with which each element of the mirror surface views the focal plane. Within the ideal image; i.e., for a diameter ratio less than 0.004, the intensity would be constant except for the effects of solar limb darkening. Following a zone of steep decline at a diameter ratio above 0.004, intensity tails off to zero at a diameter ratio of 0.0108. This tailing off is due to rays deflected by the outer regions of the mirror striking the focal plane obliquely.

The curve for 0.5 milliradians of mirror surface error is very close to the curve of zero surface error. It is about 5 percent less bright for diameter ratios less than 0.005 and a similar amount brighter for larger diameter ratios.

The curves for 1, 2, and 5 milliradians snow the strong effect of mirror surface error on the brightness at the focus. Note that with 5 milliradians of mirror surface error, the image of the sun is thoroughly smeared. The intensity of the sun's image is only about 10 percent of that for zero mirror surface error. The other 90 percent of the power is spread out beyond this area. However, even a 5 milliradian mirror may be adequate for moderate-temperature solar-energy collection.

Reradiation Loss From Absorber

Reradiation loss is a major cause of inefficiency in high temperature solar energy collection. As blackbody radiation is assumed, these losses are proportional to the area of the absorber orifice and to the fourth power of the absorber temperature. The power loss per unit area of absorber orifice is shown on figure 8. A second curve shows the energy loss per 96 min orbit. This energy loss curve assumes that the orifice is not covered during the 36 min in the shadow of the earth and is allowed to radiate to space.

Optimum Orifice Diameter

The absorber orifice admits light energy from the mirror into the absorber cavity. However, it also permits energy to escape from the cavity by radiating to space. The optimum orifice diameter maximizes the net energy input into the absorber.

The tradeoff between enlarging the orifice to admit more light energy and reducing it to prevent energy from escaping is illustrated on figure 9. This figure shows percent of power in each 0.1 percent mirror radius increment annulus for a 60° rim angle parabolic mirror with surface error standard deviation of 2.0 milliradians. This is the same curve as the curve for 2.0 milliradians

surface error plotted in figure 6. Also shown in figure 9 is power radiated at an absorber temperature of 1100 K in each 0.1 percent annulus, which increases linearly with annulus radius. The optimum orifice diameter is at the intersection of the two lines. The percentage subdivision of power can be determined directly from figure 9. As mentioned previously, 10 percent of the incident solar power was assumed absorbed by the mirror. The triangular area of collected but reradiated power represents 4 percent of the incident power. The power not captured, because the optimum orifice is too small to capture all of the reflected radiation, is 1 percent of the total. The net energy captured for this case is 85 percent of the solar radiation incident on the mirror.

Lines representing the reradiation loss at 700, 1100, 1500, and 1900 K were added to figure 6 to create figure 10. Using this figure, the optimum diameter ratio can be determined for these absorber temperatures and for mirror surface errors of 0.0, 0.5, 1.0, 2.0, and 5.0 milliradians standard deviation.

Efficiency with no Pointing Error

Solar collection efficiencies using the optimum orifice diameters determined as shown in figure 10 are plotted in figure 11. Curves of efficiency versus mirror surface error are plotted for four values of absorber temperature, 700, 1100, 1500, and 1900 K. Reradiation loss is based on 60 min of sunlight and 36 min of eclipse with the absorber orifice open. Mirror surface error is varied from 0 to 5 milliradians.

A moderate temperature, 1100 K, absorber is shown in figure 11 to have high efficiency, 75 to 89 percent, for mirror errors from 0 to 5 milliradians. Higher temperature absorbers are more sensitive to mirror accuracy because reradiation losses per unit absorber area increase with the fourth power of the absorber temperature. At 1900 K, collection efficiency falls from 83 percent at 0 milliradians mirror error to 30 percent at 5 milliradians. Thus, efficient energy collection requires a fairly accurate mirror at high temperature (0.5 milliradian for 80 percent at 1900 K), but can be achieved with a less accurate mirror at moderate temperature.

Efficiency Versus Rim Angle

As mentioned previously, rim angle is the angle formed between the axis of the mirror and a line from the focus to the rim (edge) of the mirror. Previous curves and discussion in this report assumed a 60° rim angle. This is close to optimum, but there are tradeoffs to be made. Larger rim angles bring the mirror closer to the focus for a given mirror diameter, but also cause rays from the edge of the mirror to strike the focus more obliquely.

Image intensity is plotted as a function of image radius on figure 12(a) assuming no mirror slope error and on figure 12(b) assuming standard deviation of 2 milliradians in mirror slope error. Six curves are plotted on figure 12(a) and six on figure 12(b), corresponding to six values of rim angle, 15°, 30°, 45°, 60°, 75°, and 90°. On these figures, image radius is normalized to focal length. Therefore, the difference between two curves represents the image intensity that would be contributed by the region of the mirror between

the two rim angles. Note that increases of rim angle with small rim angle;
e.g., from 15° to 30°, cause image intensity to increase almost uniformly and
image radius to increase only slightly. However, increases of rim angle with
large rim angle; e.g., from 75° to 90°, causes a smaller increase in inten-
sity, but image radius increases dramatically. The efficiencies of solar col-
lection with small rim angles is therefore reduced because of the low image
intensity, and with large rim angles, efficiency is reduced because of the
large image size.

Efficiency versus rim angle with an 1100 K absorber is plotted on
figure 13 for mirrors with standard deviations of surface error of 0. 0.5,
1.0, 2.0, and 5.0 milliradians. Accurate mirrors (0 to 1 milliradians) are
most efficient at low values (45°) of rim angle. This is shown on figure 13
to be only 0.02 or 0.03 higher than the efficiencies at 30° and 75°. Inaccu-
rate mirrors (2 to 5 milliradians) are most efficient at rim angles of about
55°. Note on figure 13 that efficiency at 30° with 5 milliradians surface
error is only three-fourths the efficiency at 55°.

Other factors in addition to maximum efficiency also influence the choice
of "optimum" rim angle. Power system configuration may be improved by increas-
ing rim angle to bring the focal point closer to the mirror. However, increas-
rim angle increases mirror curvature which may increase fabrication costs and
packaging volume. Increased packaging volume may increase transportation
costs. The ratio of mirror surface area to frontal area also increases with
increasing rim angle. This ratio plotted on figure 14 increases by almost
22 percent as rim angle increases from 0° to 90°.

In choosing optimum mirror rim angle, the energy collected by each unit
of mirror surface area may be more important that the efficiency of collecting
the intercepted sunlight. The power collected per square meter of mirror sur-
face is shown on figure 15. For accurate mirrors (0 to 1 milliradian surface
error) highest power to surface area occurs at about 30° instead of the 45°
highest efficiency rim angle that was shown on figure 13. Inaccurate mirrors
(2 to 5 milliradians) have highest power to area at 45° although highest effi-
ciency was at 55°.

Mirror Pointing Error

Ideally, the center of the focused light should be at the center of the
absorber orifice. However, due to errors of <u>alignment</u> of the mirror relative
to the absorber and of <u>pointing</u> of the mirror towards the sun, practical sys-
tems will have a total alignment and pointing error. This analysis did not
evaluate the costs associated with minimizing the error on a continuous basis
as the spacecraft orbits the earth. Also, the analysis did not evaluate the
chromatic aberration that would enlarge the image if large pointing errors
were balanced by equal and opposite alignment changes. Instead, error was
parameterized, and the effect of different error on radial distribution of
power at the absorber was determined. Future analysis could compute the costs
of maintaining these values of error and compare the costs with the effect on
distribution of power at the absorber.

Curves of radial distribution of power for 2 milliradians of mirror sur-
face error and various values of mirror alignment and pointing error are shown
on figure 16. Note that alignment and pointing errors represent errors in

8

the position of the absorber or of the sun relative to the mirror axis. Five values of error corresponding to image displacements of 0, 0.0025, 0.005, 0.0075, and 0.01 focal lengths from the center of the absorber are represented by the five curves on this figure. The largest displacement, 0.01 focal lengths, displaces the ideal image by about one solar diameter. The radial distributions of power were determined by integrating the power of the portion of the image contained in each annulus of the absorber. The curve of 0 milliradians alignment and pointing error was also shown on figure 6. Figure 16 shows that as you add alignment and pointing error there are two effects. The major effect is a shifting of the curves to larger diameter ratios as displacement increases from 0 to 0.01 focal lengths. The second, less significant, effect is a reduction in the peak value of the curves.

Efficiencies with Various Alignment and Pointing Errors

The optimum orifice diameters were recomputed to maximize efficiency with each value of image displacement. The resulting efficiencies for optimized systems with constant image displacements of 0, 0.0025, 0.005, 0.0075, and 0.01 focal lengths are plotted on figure 17. Alignment and pointing errors shift the focus of the collected energy away from the center of the absorber. This increases the optimum absorber orifice diameter, thus increasing reradiation losses and decreasing collection efficiency. The magnitude of the efficiency change varies with temperature as can be seen by comparing figure 17(a) at 700 K, figure 17(b) at 1100 K, figure 17(c) at 1500 K, and figure 17(d) at 1900 K. Each of these figures shows five curves representing image displacements of 0, 0.0025, 0.005, 0.0075, and 0.01 focal lengths. The curves show efficiency as a function of mirror surface error.

Figure 17(a) shows that with an absorber temperature of 700 K, image displacements of 0 to 0.01 focal lengths have little effect on system efficiency. It is difficult to resolve the five curves, but the top curve (greatest efficiency) represents zero alignment and pointing error, and the bottom curve represents 0.01 focal lengths of image displacement. At 1100 K on figure 17(b), there is an efficiency decrease of about 3 percent with an image displacement increase from 0.0 to 0.01 focal lengths. At 1500 K on figure 17(c), there is a greater decrease in efficiency; about 6 percent for a displacement of 0.01 focal lengths. Note also on figure 17(c) that the top curves are closely spaced, and the bottom curves are further apart. This indicates that the effect of alignment and pointing errors is nonlinear; i.e., increasing image displacement from 0 to 0.0025 focal lengths has much less effect than increasing displacement 0.0075 to 0.01 focal lengths. The curves in figure 17(d) at 1900 K also show this nonlinear effect. The decrease in efficiency at 1900 K is about 15 percent for an increase in image displacement from 0.0 to 0.01 focal lengths.

CONCLUDING REMARKS

This report describes an optical analysis of solar concentration which determined feasible collection performances and required mirror optical characteristics to achieve these performances. The analysis considered sunlight focused by a parabolic mirror into an absorber orifice with blackbody reradiation losses through this orifice. Additional analysis, including costs of achieving the optical characteristics, thermal losses associated with

transporting thermal energy from the absorber to the end use, and comparative performance of alternate power conversion systems is required to choose a specific optical design and to establish overall system feasibility.

Mirror Surface Accuracy

As highly accurate mirror surfaces and mirror tracking systems are being developed for space based telescopes, total errors much less than 1 milliradian are possible for a solar collection system. With 1 milliradian variance mirror error and 90 percent mirror reflectivity solar energy can be collected at high temperature (1100 K) and high efficiency (88 percent). Increasing mirror accuracy to obtain high efficiency reduces mirror area but may increase collector system purchase, fabrication, and launch costs. Allowing 5 milliradian variance of mirror surface error for an 1100 K collection system might reduce the overall costs even though with a 72 percent collection efficiency, the mirror would need to be about 20 percent larger than with 1 milliradian surface error and an 88 percent collection efficiency. Choosing the optimum mirror surface error thus involves a tradeoff between benefits of reduced mirror area and the increased difficulty of producing a more accurate mirror.

Absorber Radius and Rim Angle Optimization

Accurate mirrors have highest efficiency at low values (45°) of rim angle, but this is only 2 or 3 percent higher than the efficiency at any rim angle between 30° and 75°. Inaccurate mirrors (2 to 5 milliradians error) are somewhat more sensitive to rim angle. Their optimum efficiency occurs at about 55° and efficiency declines about 25 percent if the rim angle is decreased to 30° with 5 milliradians of mirror surface error.

Absorber radius interacts with the other optical parameters in determining the optimum collection system design. But if values are assigned to mirror surface error, mirror rim angle, mirror alignment and pointing error, and absorber temperature, the optimum absorber radius can be determined as follows. The optical properties of the mirror system determine the radial distribution of power at the absorber. The absorber temperature determines the radial distribution of reradiated power. The optimum absorber radius is the radius at which the incremental absorbed power equals the incremental reradiated power.

Major Results of the Analysis

1. Solar energy can be collected at high temperatures with high efficiency. For example, using a parabolic mirror of 60° rim angle that has a specular reflectivity of 0.9 and a surface error of 2 milliradians standard deviation, the net power into an absorber at 1100 K (1500 °F) is 86 percent of the solar power intercepted by the mirror.

2. Higher absorber temperatures can be achieved at lower efficiencies or higher efficiencies can be achieved at lower temperatures. Both temperature and efficiency can be increased by increasing mirror surface accuracy and/or mirror spectral reflectivity.

3. Collection efficiency is near its maximum level across a broad plateau of rim angles from 40° to 70°. At lower rim angles, the cause of reduced efficiency is an increase in distance from the mirror to its focus; at higher rim angles, efficiency falls off because rays from the mirror's rim impinge on the focal plane at grazing angles.

REFERENCES

1. Angström, A.K.; and Angström, K.H.: The Distribution of Radiation Over the Sun's Disk. Sol. Energy, vol. 13, no. 2, 1971, pp. 243-250.

2. Curran, D.G.T.; and Millard, J.M.: Results of Contamination/Degradation Measurements on Thermal Control Surfaces of an Operational Satellite. AIAA Paper 77-740, June 1977.

3. Lowi, A: Solar Dynamic Power Systems Study - Volume II: Solar Dynamic Power Systems Evaluation. SSD-TDR-63-115, Vol. II, Aerospace Corp., Sept. 15, 1965. (AD-474138)

4. Hamadto, S.A.: Planar-Sectioned Solar Concentrators. 1: Polygon Reflectors. Appl. Opt., vol. 23, no. 8, Apr. 15, 1984, pp. 1279-1283.

5. Wetherell, W.B.; and Rimmer M.P.: General Analysis of Aplanatic Cassegrainian, Gregorian, and Schwarzschild Telescopes. Appl. Opt., vol. 11, no. 12, Dec. 1972, p. 2817-2832.

6. Rabl, Ari: Comparison of Solar Concentrators. Sol. Energy, vol. 18, no. 2, 1976, pp. 93-111.

7. Horne, W.E.; et al.: "Solar Thermophotovoltaic Space Power System. Energy to the 21st Century, Vol. 1, AIAA, 1980, pp. 377-382.

8. McDanal, A.J : Optical Analysis of Paraboloidal Solar Concentrators with Secondary Reflectors. Sun II - Proceedings of the International Solar Energy Society. K.W. Boer and B.H. Glenn, eds., Pergamon, 1969, pp. 1256-1260.

9. Mihora, Dennis J.; and Redmond, Peter J.: Electrostatically Formed Antennas. J. Spacecr. Rockets, vol. 17, no. 5, Sept.-Oct. 1980, pp. 465-473.

10. Analysis of Solar Reflectors Mathematical Theory and Methodology for Error Model Synthesis from Experimental Ray Trace Data. EDR-3958, General Motors Corp., Indianapolis, IN, Sept. 1, 1964.

11. Solar Parabolic Dish Technology Annual Evaluation Report.(JPL-PUB-84-25, Jet Propulsion Lab; NASA Contract NAS7-819) NASA CR-173725. 1984.

12. Truscello, V.C.: The Parabolic Concentrating Collector - A Tutorial. (JPL-PUB-79-7, Jet Propulsion Lab; NASA Contract NAS7-100) NASA CR-158426, 1979.

13. Roschke, John E.; and Wen, L.: Preliminary Systems Definition Study for Solar Thermal Dynamic Space Power Systems. Oct. 1984. (Unpublished Report Prepared for NASA Headquarters and Lewis Research Center)

14. Wen, L.: Thermal Optical Surface Properties and High Temperature Solar Energy Conversion. AIAA Paper 78-903, May 1978.

15. Wen, L.; et al.: Comparative Study of Solar Optics for Paraboloidal Concentrators. ASME Paper 79-WA/SOL-8, Dec. 1979.

16. Jaffe, Leonard: Optimization of Dish Solar Collectors. J. Energy, vol. 7, no. 6, 1983, pp. 684-694.

17. Solar Dynamic Systems Symposium, Proceedings. Interagency Advanced Power Group, Washington, D.C., 1963.

18. English, Robert E.: Technology for Gas-Turbine Space-Power Plants Using Solar and Nuclear Energy. Unpublished Report.

19. Jack, John R.; Spisz, Ernie W.; and Cassidy, John F.: The Effect of Rocket Plume Contamination on the Optical Properties of Transmitting and Reflecting Materials. AIAA Paper 72-56, Jan. 1972.

20. Kaykaty, Gabriel: Analysis of Performance of Double-Reflector System for Collecting Solar Energy. NASA TN-D-3534, 1966.

21. Kerslake, William R.: Status of SERT II Thrusters and Spacecraft - 1976. AIAA Paper 76-1061, Nov. 1976.

22. Mroz, Thaddeus S.; and King, Robert B.: Polymer-Film Coating of Magnesium for Paraboloidal Mirrors. NASA TN-D-4734, 1968.

23. Richter, Carl W.; et al.: Design and Fabrication of a Low-Specific-Weight Para- bolic Dish Solar Concentrator. NASA TP-1152, 1978.

24. Smith, Robert E.; and West, George S.: Space and Planetary Environment Guidelines for Use in Space Vehicle Development, vol. 1, 1982 Revision. NASA TM-82478, 1983, pp. 1-11.

25. Canning, John S.: The Winston Solar Concentrator Described as an Ellipse. Sol. Energy, vol. 18, no. 2, 1976, pp. 155-156.

26. Singh, Parmpal; and Cheema, L.S.: Performance and Optimization of a Cylindrical-Parabola Collector. Sol. Energy, vol. 18, no. 2, 1976, pp. 135-141.

27. Leonard, James A.: Solar Thermal Parabolic Dish Technology and Applications. Advanced Energy Systems, Their Role in Our Future, vol. 3, Proceedings, 19th Intersociety Energy Conversion Engineering Conference, American Nuclear Society, 1984, pp. 1681-1685.

28. Pettit, R.B.; Vittitoe, C.N.; and Biggs, F.: Simplified Calculational Procedure for Determining the Amount of Intercepted Sunlight in an Imaging Solar Concentrator. J. Solar Energy Eng., vol. 105, no. 1, Feb. 1983, pp. 101-107.

29. Carlson, D.E.E.; Diver, R.B.; and Fletcher, E.A.: A Simple Model for Predicting the Flux Distribution Through the Focal Plane of a Multifaceted-Concentrator Solar Furnace. J. Solar Energy Eng., vol. 106, no. 1, Feb. 1984, pp. 103-105.

30. Liu, B.Y.H.; and Jordan, R.C.: Performance and Evaluation of Concentrating Solar Collectors for Power Generation. J. Eng. Power, vol. 87, ro. 1, Jan. 1965, pp. 1-7.

31. Lumsdaine, Edward; and Cherng, J.C.: On Heat Exchangers Used with Solar Concentrators. Sol. Energy, vol. 18, no. 2, 1976, pp. 157-158.

32. Duffie, John A.; and Beckman, William A.: Solar Energy Thermal Processes. Wiley, 1974.

33. Hedgepeth, L.M.; Huffman, G.D.; and Ostdiek, F.R.: Comparison of Weights and Performances of Solar Dynamic Energy Conversion Systems. AFAPL-TR-64-44, Air Force Aero Propulsion Lab, Sept. 1965. (AD-476940)
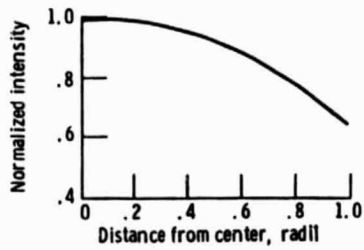
Figure 1. - Solar intensity varia-
tion, limb darkening.
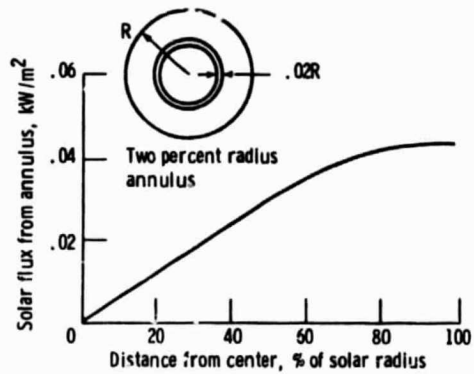
Figure 2. - Solar flux from each 2% radius annulus.
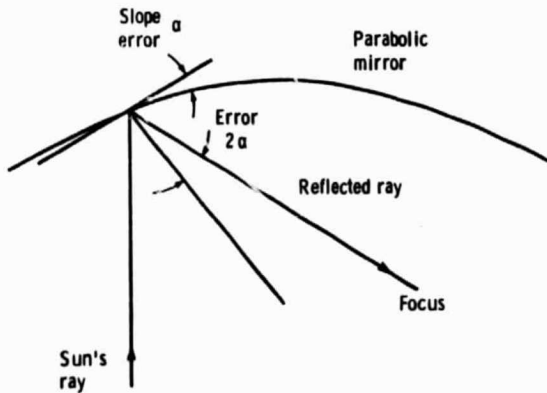
Figure 3. - Error in reflected ray is twice surface slope error.
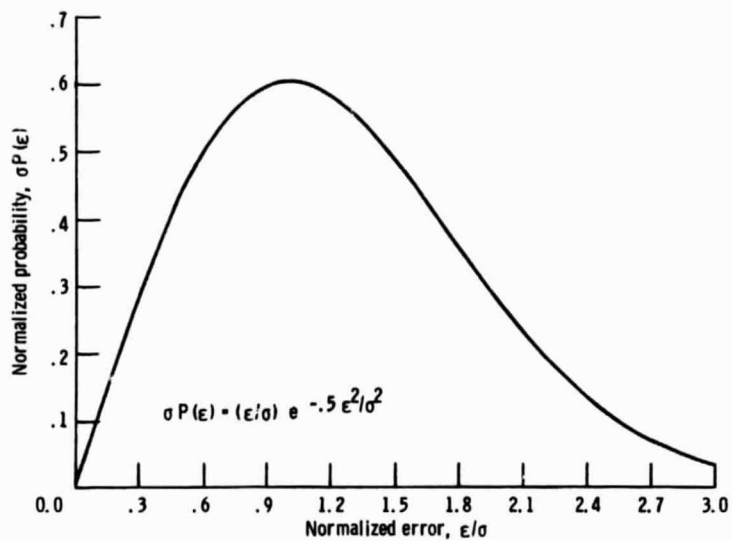
Figure 4. - Two dimensional normal probability distribution of mirror slope errors.

$$\sigma P(\varepsilon) = (\varepsilon/\sigma) \, e^{-.5 \, \varepsilon^2/\sigma^2}$$
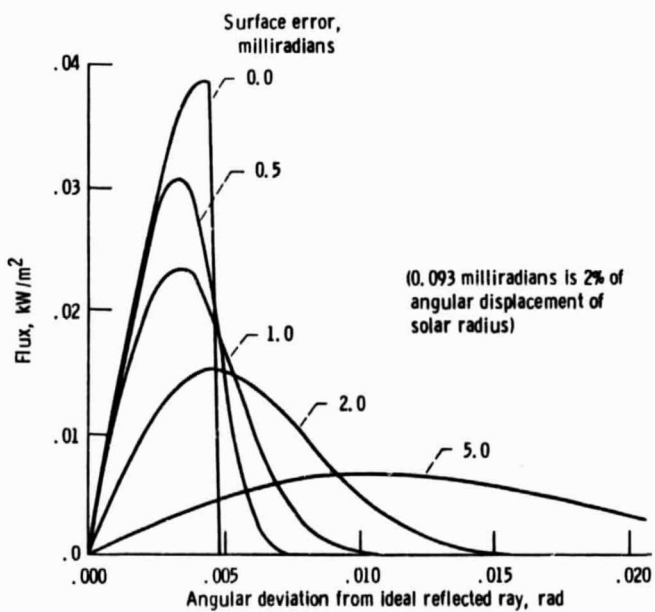
Figure 5. - Reflected flux in each 0.093 milliradian annulus.
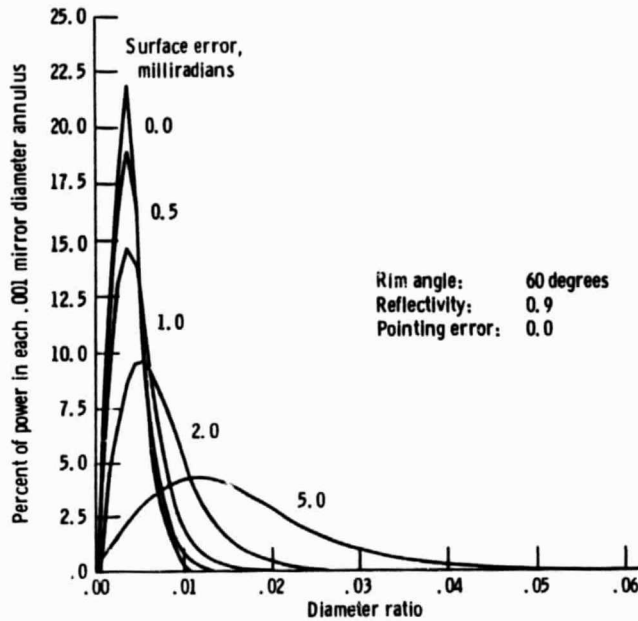
Figure 6. – Radial distribution of power at focus.
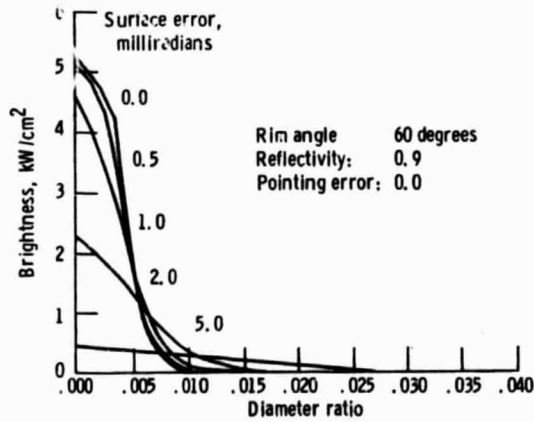
Figure 7. – Brightness of annular regions of focus.
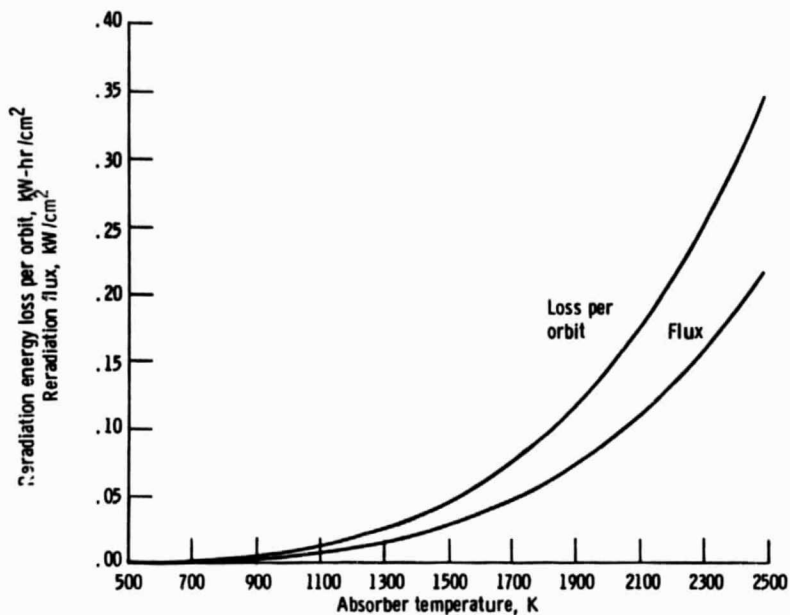
Figure 8. - Reradiation loss from absorber.
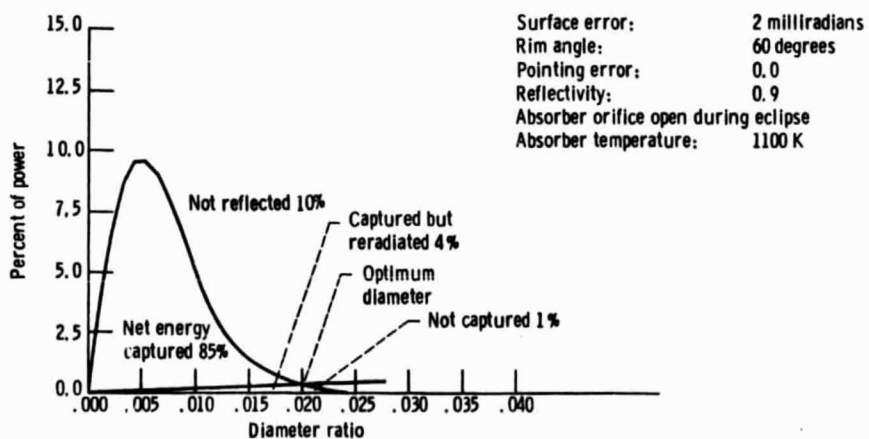
Figure 9. - Optimum orifice diameter.
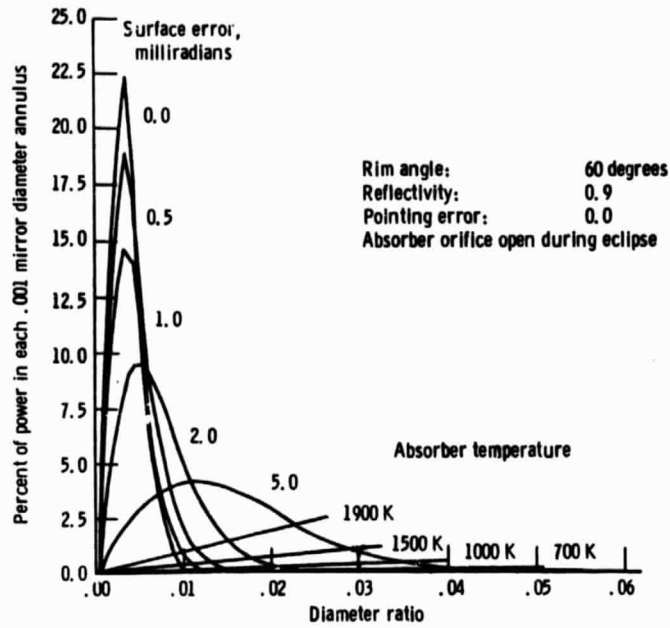
Figure 10. - Energy captured at various mirror accuracies and absorber temperatures.
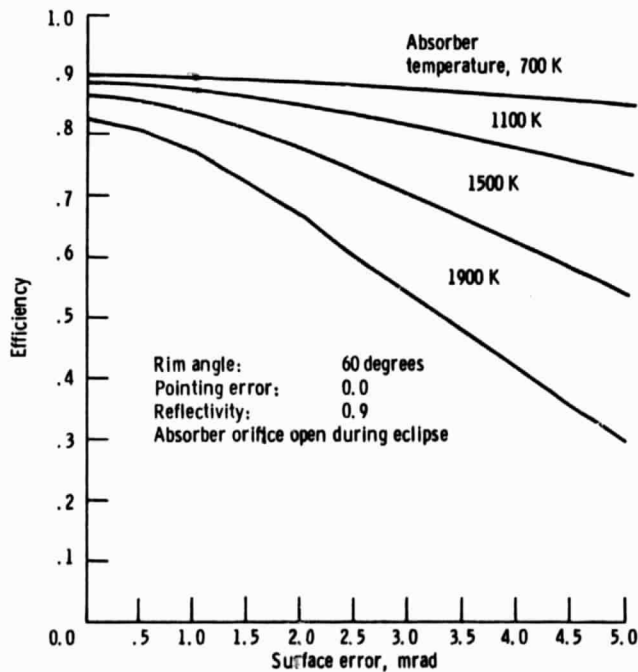
Figure 11. - Efficiency vs mirror error with optimum absorber diameter.
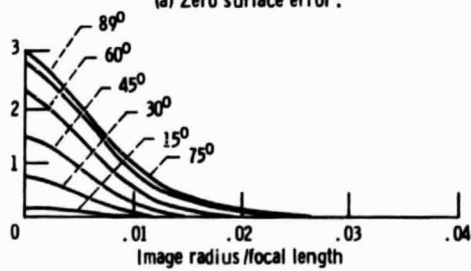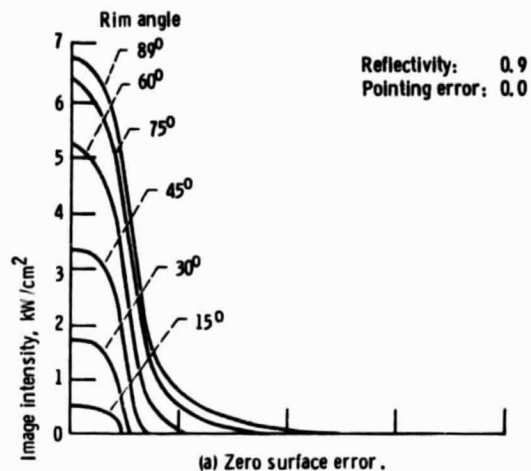
Figure 12. – Image intensity for various rim angles.
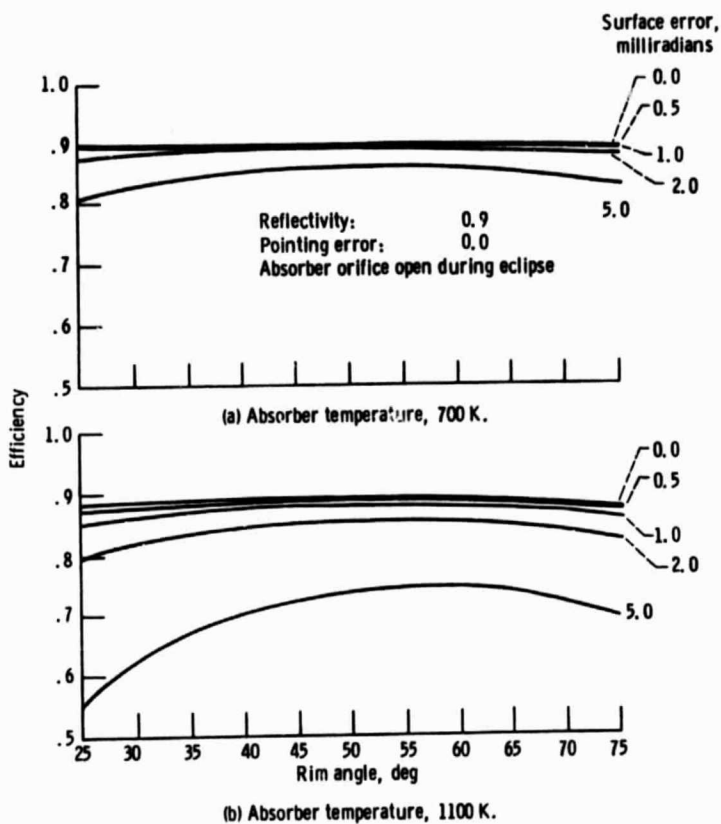
Figure 13. - Collection efficiency as a function of rim angle at various absorber temperatures.
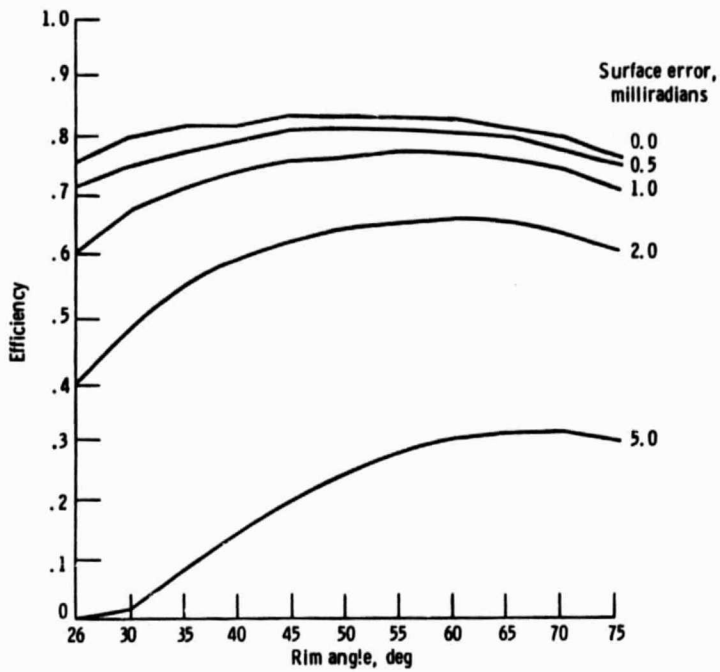
(c) Absorber temperature, 1500 K.

Figure 13. - Continued.
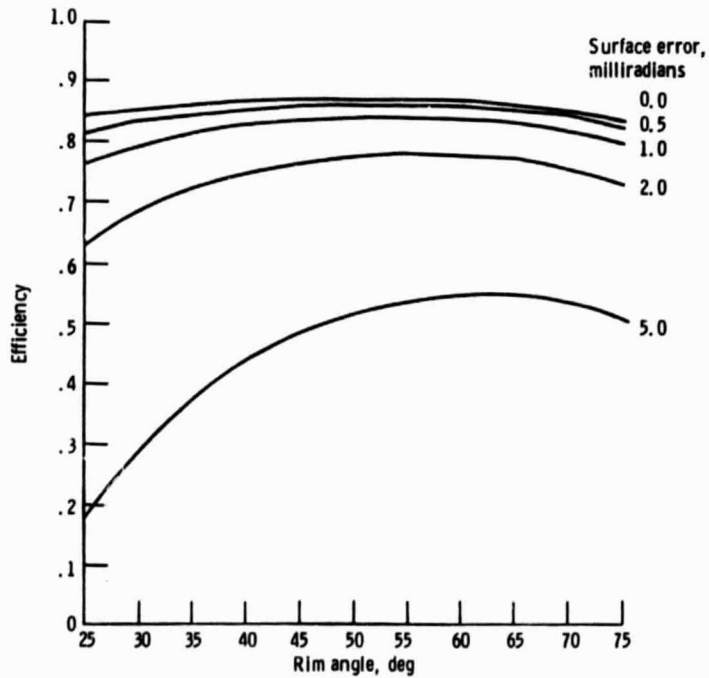
(d) Absorber temperature, 1900 K.
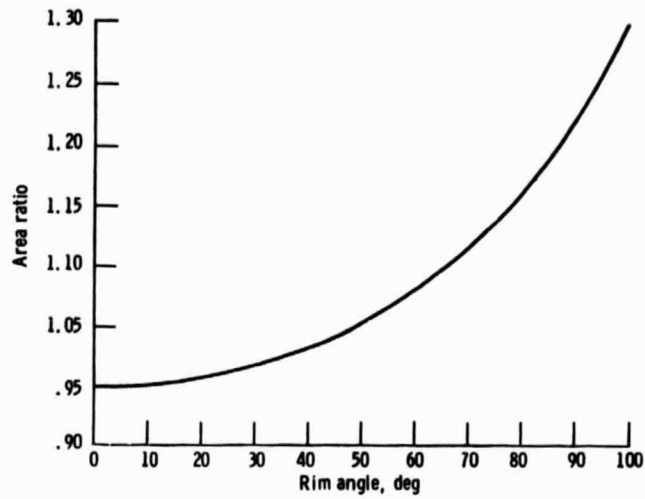
Figure 13. - Concluded.

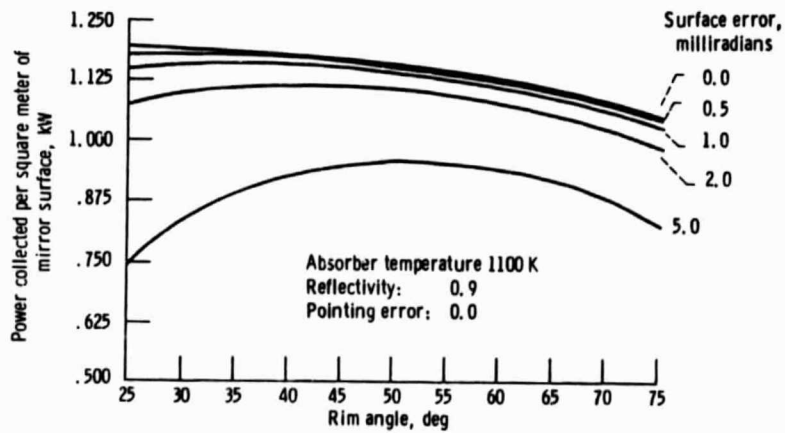Figure 14. - Ratio of parabolic mirror surface area to frontal area.

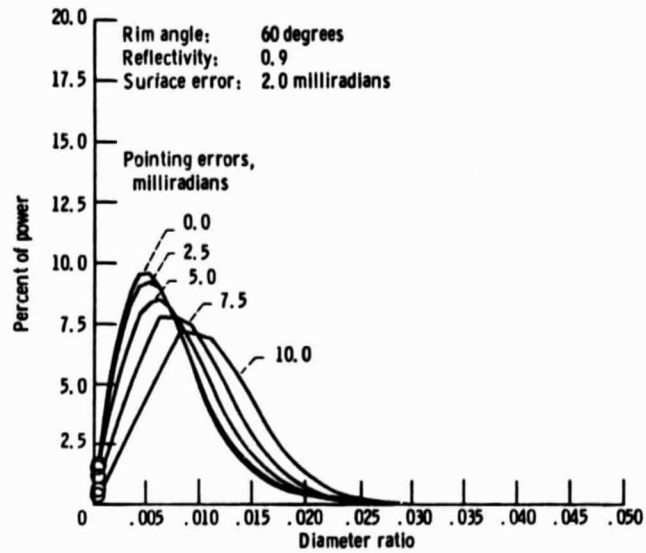Figure 15. - Power collected per square meter of mirror surface as a function of rim angle.

Figure 16. - Effect of mirror pointing error on distribution of power on the focal plane.
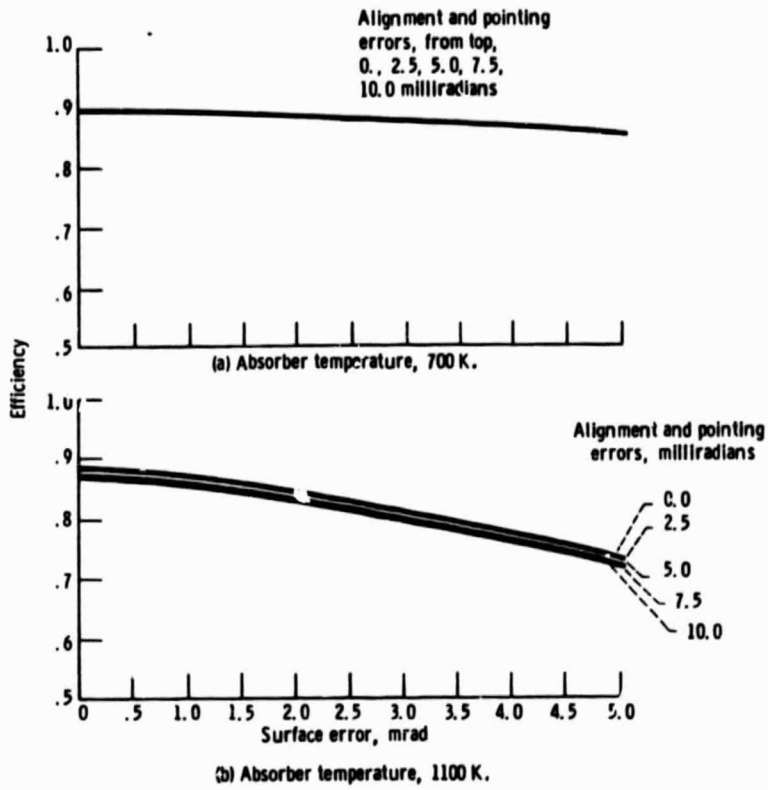
Figure 17. - Efficiency vs mirror surface error with various align-
ment and pointing errors. Rim angle, 60 degrees; reflectivity: 0. 9;
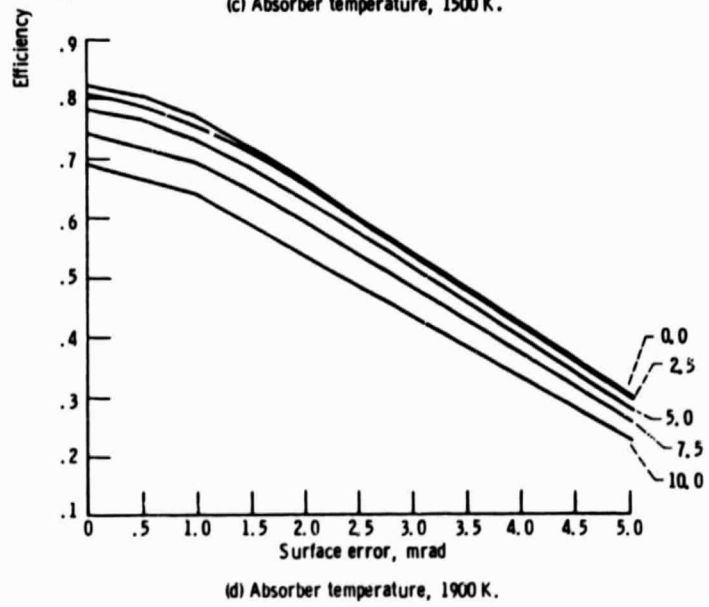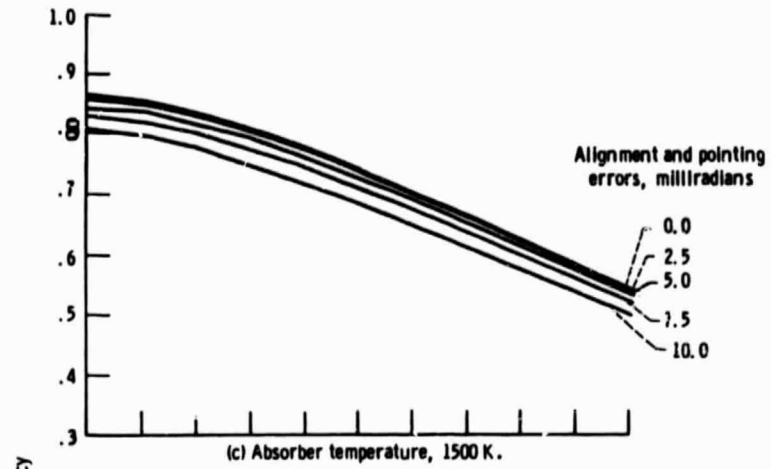absorber orifice open during eclipse.

(c) Absorber temperature, 1500 K.

(d) Absorber temperature, 1900 K.

Figure 17. - Concluded.

1. Report No. NASA TM-87080	2. Government Accession No.	3. Recipient's Catalog No.
4. Title and Subtitle Optical Analysis of Parabolic Dish Concentrators for Solar Dynamic Power Systems in Space		5. Report Date August 1985
		6. Performing Organization Code 482-55-62
7. Author(s) Kent S. Jefferies		8. Performing Organization Report No. E-2659
		10. Work Unit No.
9. Performing Organization Name and Address National Aeronautics and Space Administration Lewis Research Center Cleveland, Ohio 44135		11. Contract or Grant No.
		13. Type of Report and Period Covered Technical Memorandum
12. Sponsoring Agency Name and Address National Aeronautics and Space Administration Washington, D.C. 20546		14. Sponsoring Agency Code

15. Supplementary Notes

16. Abstract

An optical analysis of a parabolic solar collection system operating in earth orbit was performed using ray tracing techniques. The analysis included the effects of: (1) solar limb darkening, (2) parametric variation of mirror surface error, (3) parametric variation of mirror rim angle, and (4) parametric variation of alignment and pointing error. This ray tracing technique used numerical integration to combine the effects of rays emanating from different parts of the sun at different intensities with the effects of normally distributed mirror-surface errors to compute the angular intensity distribution of rays leaving the mirror surface. A second numerical integration was then performed over the surface of the parabolic mirror to compute the radial distribution of brightness at the mirror focus. Major results of the analysis included: (1) solar energy can be collected at high temperatures with high efficiency, (2) higher absorber temperatures can be achieved at lower efficiencies, or higher efficiencies can be achieved at lower temperatures, and (3) collection efficiency is near its maximum level across a broad plateau of rim angles from 40° to 70°.

17. Key Words (Suggested by Author(s)) Optical analysis; Parabolic dish; Parabolic reflectors; Solar collectors; Solar dynamic; Space power; Ray tracing; Space station	18. Distribution Statement Unclassified - unlimited STAR Category 20	
19. Security Classif. (of this report) Unclassified	20. Security Classif. (of this page) Unclassified	21. No. of pages	22. Price*